Clays and Clay Minerals, Vol. 51, No. 2, 186–196, 2003.

THE DESTRUCTIVE ROLE OF DIFFUSION ON CLAY MEMBRANE BEHAVIOR

CHARLES D. SHACKELFORD* AND JAE-MYUNG LEE
Department of Civil Engineering, Colorado State University, Fort Collins, CO 80523-1372, USA

Abstract—The results of a combined chemico-osmotic/diffusion experiment conducted on a geosynthetic clay liner (GCL) containing Na-bentonite illustrate the destructive role of diffusion on the ability of the GCL to act as a semipermeable membrane. The experiment is conducted by maintaining a concentration difference of 5 mM $CaCl_2$ across the GCL specimen while preventing the flow of solution through the specimen. A time-dependent membrane efficiency is derived from measured pressure differences induced across the specimen in response to the applied concentration difference. The diffusive mass fluxes of the solutes (Cl^- and Ca^{2+}) through the specimen are also measured simultaneously. An initial increase in induced pressure difference across the specimen to a peak value of 19.3 kPa is observed, followed by a gradual decrease to zero. The decrease in induced pressure difference is consistent with compression of diffuse double layers between clay particles and particle clusters due to diffusion of Ca^{2+}, resulting in a concomitant increase in pore sizes and decrease in the observed membrane behavior. The time required for effective destruction of the initially observed semipermeable membrane behavior correlates well with the time required to achieve steady-state Ca^{2+} diffusion. The results have important implications for the ability of clays to sustain membrane behavior.

Key Words—Chemico-osmotic Efficiency, Clay Membrane, Diffuse Double Layer, Diffusion, Membrane Behavior, Reflection Coefficient, Solute Restriction.

INTRODUCTION

Solute restriction resulting from the existence of membrane behavior in clays has been shown to influence volume change behavior, cause apparent deviations from Darcy's law in hydraulic conductivity testing, generate anomalous pore-water pressures in low-permeability geologic formations, and affect the rate of solute migration through low-permeability clays (Malusis and Shackelford, 2002a). Restricted solute migration resulting from membrane behavior is also currently being considered in the context of clay containment barriers for geoenvironmental applications, such as aquitards and engineered clay liners for containment of disposed waste, and vertical cutoff walls (*e.g.* soil-bentonite walls) for *in situ* containment of contaminated groundwater (*e.g.* Keijzer and Loch, 2001; Malusis *et al.*, 2001a; Shackelford *et al.*, 2001). In such cases, the existence of membrane behavior may be important in terms of evaluating the hydraulic and contaminant transport performance of the containment barrier, since the primary objective of the barrier is to maintain a contaminant concentration at the outer boundary of the barrier that is lower than the source concentration of the same contaminant. For example, in the case where the clay containment barrier acts as a semipermeable membrane, both chemico-osmotic counter flow and contaminant (solute) restriction would act to reduce the outward contaminant flux (Malusis *et al.*, 2001a; Shackelford *et al.*, 2001). Thus, a clay containment barrier that behaves as a semipermeable membrane is expected to perform better than one that does not exhibit membrane behavior.

In the case of electrolyte solutions, membrane behavior in clays generally is attributed to electrostatic repulsion of the ions by electric fields associated with the diffuse double layers (DDLs) of adjacent clay particles (*e.g.* Hanshaw and Coplen, 1973; Fritz, 1986). Thus, the factors that tend to cause an increase in the thickness of DDLs (*i.e.* at constant porosity), such as decreasing ion concentration and/or decreasing ion valence, also tend to enhance the membrane efficiency of clays that behave as semipermeable membranes (see Kemper and Rollins, 1966; Kemper and Quirk, 1972). However, an increasing ion concentration and/or ion valence also may result in a reduction in membrane efficiency.

For example, Barbour (1986) and Barbour and Fredlund (1989) attributed expulsion of pore-water from specimens in chemico-osmotic consolidation tests due to diffusion of high-concentration salts into the soil specimen and subsequent 'collapse' of the DDLs. Whitworth and Fritz (1994) correlated reductions in membrane efficiency of compacted smectitic membranes during forced passage of a 10 mM NaCl solutions through the membranes to compression of DDLs reflected by changes in the permeability of the membranes.

Malusis *et al.* (2001b) and Malusis and Shackelford (2002a) observed partial time-dependent decreases in membrane efficiency for thin specimens (8–13 mm) of a geosynthetic clay liner (GCL) containing Na-bentonite

* E-mail address of corresponding author:
shackel@engr.colostate .edu
DOI: 10.1346/CCMN.2003.0510209

Copyright © 2003, The Clay Minerals Society

https://doi.org/10.1346/CCMN.2003.0510209 Published online by Cambridge University Press

subjected to differences in KCl concentrations. For example, the induced pressure difference for a test with a concentration difference of 47 mM KCl increased to ~40 kPa after ~3 days, but subsequently decreased before reaching a steady value of 32 kPa. This time-dependent decrease in membrane efficiency tended to increase with increasing KCl concentration, and/or increasing specimen porosity (Malusis and Shackelford, 2002a). Malusis *et al.* (2001b) and Malusis and Shackelford (2002a) concluded that the observed behavior was consistent with expected behavior based on compression of DDLs resulting from increases in KCl concentrations due to solute diffusion in their closed-system (no-flow) testing apparatus.

However, apparent reductions in membrane efficiency have not always been attributed to collapse of DDLs due to increased solute concentrations within the clay membrane. For example, Keijzer *et al.* (1997, 1999) attributed changes in induced chemico-osmotic pressures across compacted Na-bentonite specimens located between fresh- and salt-water reservoirs to time-dependent changes in the boundary salt concentrations, resulting in a time-dependent decrease in the concentration gradient across the specimen. These boundary concentration changes were attributed to the net migration of water in a direction of decreasing concentration gradient due to the process of diffusion osmosis (Olsen *et al.*, 1990). As a result, Keijzer *et al.* (1997, 1999) concluded that the decrease in observed pressure difference did not necessarily correlate with a decrease in membrane efficiency of the specimens.

The results of the aforementioned studies suggest that migrating solutes may adversely affect the efficiency of clay membranes. However, these previous studies were not performed with the specific purpose of evaluating the potential effect of diffusion on clay membrane efficiency. In addition, differences among the studies in terms of testing objectives (*e.g.* consolidation *vs.* membrane efficiency) and testing approaches (*e.g.* open systems *vs.* closed systems, constant *vs.* time-dependent boundary conditions) have precluded any consensus with respect to the potential effect of diffusion of invading solutes on clay membrane efficiency. As a result, the objective of this paper is to illustrate a direct correlation between diffusion of invading solutes and the destruction of the efficiency of a semipermeable clay membrane. This objective is achieved using a unique testing apparatus that maintains constant boundary concentrations while preventing solution flow through the specimen, thereby eliminating the potential effects of changes in boundary concentrations and transport processes other than diffusion (*e.g.* chemico-osmosis, diffusion-osmosis) from consideration. The results of this evaluation may have significant ramifications with respect to use and performance of clay membranes as barriers for geoenvironmental containment applications.

MATERIALS AND METHODS

Materials

The Bentonfix® NS GCL (Terrafix Geosynthetics, Inc., Toronto, Ontario, Canada) was used in this study. A schematic cross-section of this GCL is shown in Figure 1. The GCL consists of a layer of Na-bentonite sandwiched between woven and non-woven polypropylene geotextiles held together by needle-punched fibers. The GCL is ~6 mm thick in an air-dried condition, but quickly swells to 10–15 mm upon exposure to water when unconfined. The bentonite content of the GCL measured in accordance with ASTM D 5993 is 5.1 kg/m^2. The mineralogy, exchangeable metals, and cation exchange capacity (CEC) for the bentonite portion of the GCL are given in Table 1.

Although the GCL used in this study is not from the same manufacturer as the GCL used by Malusis *et al.* (2001b) and Malusis and Shackelford (2002a,b), the components of the GCL and the mineralogical composition of the bentonite in the two GCLs are very similar. This similarity was considered important because the GCL used by Malusis *et al.* (2001b) and Malusis and Shackelford (2002a,b) was shown to behave as a semipermeable membrane in the presence of KCl solutions ranging from 3.9 to 47 mM for specimen thicknesses ranging from 8 to 13 mm, with greater membrane efficiencies associated with lower KCl concentrations and/or thinner GCL specimens. As a result, the GCL used in this study was expected to exhibit semipermeable membrane behavior, *i.e.* provided the boundary salt concentration was suitably low and the specimen was suitably thin.

The liquids used in the experiment consist of tap water that is processed to remove ions by passage through three Barnstead® ion-exchange columns in series (electrical conductivity, EC, at 25°C = 0.30 mS/m, pH = 5.45), and a 5 mM calcium chloride ($CaCl_2$) solution (EC = 121 mS/m, pH = 5.58) prepared by dissolving $CaCl_2$ (powdered, >96% pure, Sigma-Aldrich Co., St. Louis, Missouri) in the processed tap

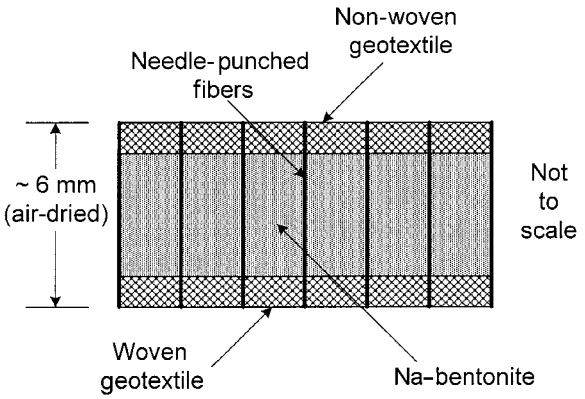


Figure 1. Schematic cross-section of geosynthetic clay liner used in this study.

https://doi.org/10.1346/CCMN.2003.0510209 Published online by Cambridge University Press

Table 1. Properties of bentonite in a geosynthetic clay liner.

Property	Standard	Value
Principal minerals (%)	a	
Montmorillonite		78
Cristobalite		9
Plagioclase feldspar		4
Quartz		3
Tridymite		2
Others		4
Cation exchange capacity (meq/100 g)	b	69.4
Exchangeable cations (meq/100 g)	b	
Ca		13.9
Mg		4.4
Na		48.1
K		0.7
Sum		67.1
Soluble cations (mg/kg)	b, c	
Ca		241
Mg		29
Na		3437
K		51
Soil pH	b, d	8.9
Electrical conductance (mS/m) @ 25°C	b, d	300

[a] Based on XRD analyses performed by Mineralogy Inc., Tulsa, Oklahoma
[b] Based on procedures described in Shackelford and Redmond (1995)
[c] Measured from a 1 g:20 mL clay-water extract
[d] Measured on saturated soil paste

water. The $CaCl_2$ was selected for use in this study to determine if the GCL would exhibit membrane behavior when exposed to the divalent Ca^{2+} cation, as opposed to the previous studies that used the monovalent K^+ cation, and the 5 mM concentration was thought to be sufficiently low to enhance the possibility of observing membrane behavior.

Testing apparatus

The testing apparatus and testing procedures are the same as described by Malusis *et al.* (2001b), and Malusis and Shackelford (2002a,b); therefore, only a relatively brief description is provided here. A schematic illustration of the testing apparatus is shown in Figure 2.

The testing cell consists of a rigid acrylic cylinder, top piston and base pedestal. The top piston is locked in place to prevent soil expansion and to control the thickness (porosity) of the soil specimen. Solutions containing initial concentrations of a given electrolyte (designated as C_{ot} and C_{ob} in Figure 2) are expelled from each of the two actuators (syringes) at the same constant rate via the plunger that is attached to a flow-pump drive (not shown), and subsequently are infused through the porous stones across the top and bottom boundaries of the specimen. Circulation outflow from these boundaries is simultaneously collected through the opposite end of the actuator at the same rate in order to maintain a constant volume inside the testing cell (*i.e.* $\Delta V_{cell} = 0$) and prevent liquid flux through the specimen. Under these conditions, the chemico-osmotic efficiency coefficient, ω, also commonly known as the reflection coefficient, σ, is defined as follows (Staverman, 1952; Katchalsky and Curran, 1965; Groenevelt and Elrick, 1976; van Oort *et al.*, 1996; Malusis *et al.*, 2001b):

$$\omega = \frac{\Delta P}{\Delta \pi} \tag{1}$$

where ΔP = the measured pressure difference induced across the specimen as a result of prohibiting chemico-osmotic flux of solution, and $\Delta\pi$ = the theoretical chemico-osmotic pressure difference across an 'ideal' semipermeable membrane (*i.e.* $\omega = 1$) subjected to an applied difference in solute concentration (*e.g.* Olsen *et al.*, 1990).

The value for $\Delta\pi$ in equation 1 is calculated based on the salt concentrations at the specimen boundaries in accordance with the van't Hoff expression as follows (Malusis *et al.*, 2001b; Malusis and Shackelford, 2002a):

$$\Delta \pi = RT\sum_{i=1}^{N}(C_{ob,i} - C_{ot,i}) \tag{2}$$

where R = the universal gas constant [8.314 J mol $^{-1}$K^{-1}], T = the absolute temperature [K], $C_{ob,i}$ = the initial concentration of solute species i at the bottom of the specimen [mol L^{-3}], $C_{ot,i}$ = the initial concentration of solute species i at the top of the specimen [mol L^{-3}], and N = the total number of solute species. For simple salt solutions, such as $CaCl_2$, equation 2 may be written more conveniently as:

$$\Delta \pi = \nu RT\Delta C \tag{3}$$

where ν = the number of ions per molecule of the salt, and ΔC (= $C_{ob} - C_{ot}$) = the salt concentration gradient.

The induced pressure difference, ΔP, in equation 1 is measured using a differential pressure transducer that is located as shown in Figure 2. Typical trends in the induced pressure difference as a function of time based on the data reported by Malusis *et al.* (2001b) and Malusis and Shackelford (2002a) are illustrated schematically in Figure 3a. The observed effect of increasing solute concentration difference on the post-peak pressure difference previously described is also illustrated in Figure 3a.

The differences in solute (Cl^- and Ca^{2+}) concentrations between the top and bottom boundaries of the specimen also cause solute diffusion from the higher concentration boundary (top) to the lower concentration boundary (bottom), such that a steady-state solute flux through the bottom of the specimen is eventually established and maintained. This scenario is commonly referred to as the steady-state approach for diffusion testing (Shackelford, 1991).

https://doi.org/10.1346/CCMN.2003.0510209 Published online by Cambridge University Press

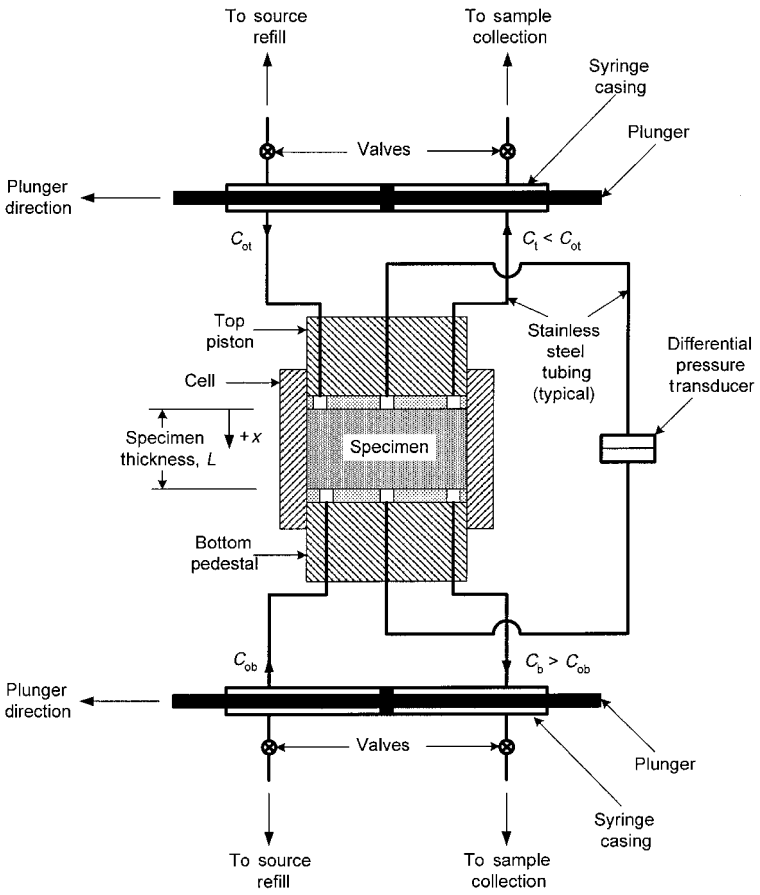


Figure 2. Schematic cross-section of test cell (re-drawn after Malusis and Shackelford, 2002a).

In the steady-state approach, the measured concentrations for a given solute in the circulation outflow (*i.e.* from the base pedestal) are typically converted to cumulative mass per unit area, Q_t, using the following expression (Malusis *et al.*, 2001b):

$$Q_t = \frac{1}{A}\sum_{i=1}^{N_s} \Delta m_i = \frac{1}{A}\sum_{i=1}^{N_s} C_{b,i}\Delta V_i \qquad (4)$$

where A = cross-sectional area of the specimen, Δm_i = the incremental mass of the solute species collected over a time increment (Δt), $C_{b,i}$ = the concentration of the solute species in the incremental volume, ΔV_i, of circulation outflow from the base pedestal corresponding to the same Δt, and N_s = the number of incremental samples corresponding to the total elapsed time, t. The results are plotted in terms of Q_t *vs.* t, as illustrated schematically in Figure 3b. The curved portion of the example plot in Figure 3b represents transient diffusion, while the linear portion of the data in Figure 3b corresponding to the constant slope, $\Delta Q_t/\Delta t$, represents steady-state diffusion.

Two characteristic times also are associated with the plot in Figure 3b. First, the time corresponding to the intersection of the extension of the steady-state slope to the x axis is referred to as the time lag, t_L (Shackelford, 1991). The value of t_L can be used to determine the retardation factor, R_d, which reflects the adsorption behavior of the solute during transient diffusion (see Malusis *et al.*, 2001b). Second, the time corresponding to the intersection of the initial curved portion of the example plot shown in Figure 3b, representing the transient diffusion stage, and the linear portion of the example plot, representing steady-state diffusion, is the time required to achieve steady-state diffusion, t_{ss}. Note that t_{ss} is always greater than t_L, and that t_{ss} typically is not evaluated when steady-state diffusion tests are performed.

The effective diffusion coefficient, D^*, of the given solute species is determined from the slope of the steady-state portion of the response, $\Delta Q_t/\Delta t$, in accordance with the following expression:

$$D^* = -\left\{\frac{\Delta Q_t}{\Delta t}\right\}\left\{\frac{L}{n\Delta C}\right\} \qquad (5)$$

where n = the specimen porosity and L = the specimen thickness. As noted by Malusis and Shackelford (2002b), the value of D^* determined according to equation 5 is a

https://doi.org/10.1346/CCMN.2003.0510209 Published online by Cambridge University Press

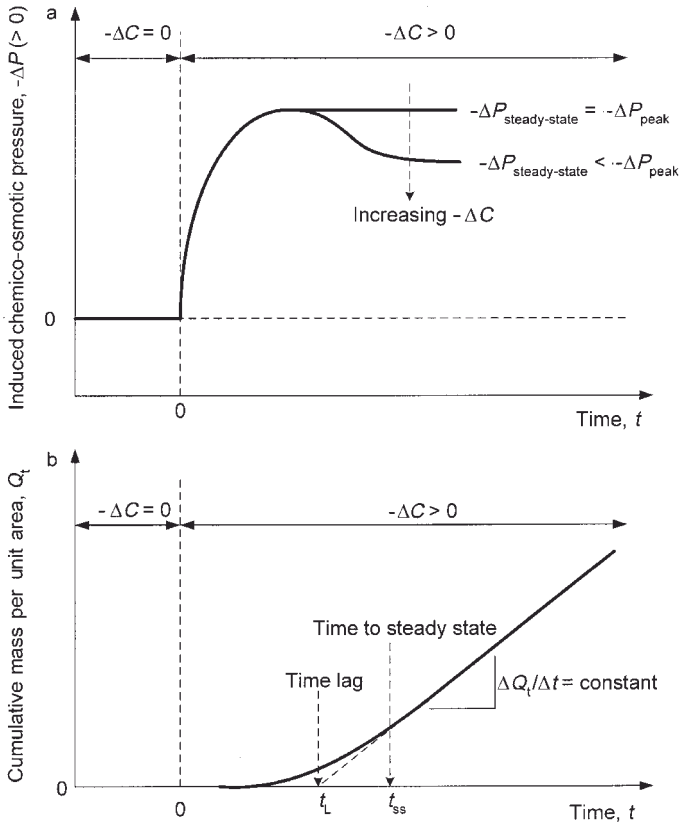


Figure 3. Schematic illustration of typical results obtained from combined chemico-osmotic/diffusion experiments: (a) trends in induced chemico-osmotic pressure observed for clay membranes; and (b) trends in cumulative solute mass through specimen due to diffusion.

coupled effective diffusion coefficient that includes a coupling term associated with the prevention of solution flow in accordance with the principles of irreversible thermodynamics. In the limit, as the membrane efficiency of a clay approaches zero, the coupled effective diffusion coefficient given by equation 5 converges to the true effective diffusion coefficient represented by Fick's first law for diffusion in soil as defined by Shackelford and Daniel (1991).

Specimen assembly and disassembly

A circular specimen of the GCL with a nominal diameter of 71.1 mm was cut from a larger GCL sheet, and placed on the base pedestal inside the testing cell. The cylinder then was filled with processed tap water to submerge the specimen, and the top piston was lowered into the cylinder to compress the GCL to a thickness of ~5 mm to enhance the potential for membrane behavior. After compression, the top piston was locked in place to prevent further volume expansion of the specimen during the test due to swelling of the bentonite.

The initial concentrations of the soluble cations in the pore-water of the specimen based on the measured soluble cations concentrations shown in Table 1, the assumption of 100% saturation, and a measured porosity of the specimen of 0.718, were ~164 mM for Na, 6.6 mM for Ca, 1.4 mM for K and 1.3 mM for Mg. Since the sum of these cation concentrations far exceeds the concentration of the source solution (*i.e.* 5 mM $CaCl_2$), the specimen was permeated under backpressure with processed tap water before testing to saturate the specimen and to enhance the potential for membrane behavior by removing soluble salts. This permeation was continued until the electrical conductivity, EC, of the effluent from the specimen was ~50% of the measured EC for the 5 mM $CaCl_2$ source solution of 121 mS/m, as shown in Figure 4.

After permeation, the processed tap water was circulated at the top and bottom boundaries of the specimen for ~5 days to establish a steady baseline differential pressure (see Malusis *et al.*, 2001b). The chemico-osmotic/diffusion portion of the experiment then was initiated by circulating the 5 mM $CaCl_2$ solution in the top piston (*i.e.* $C_{ot} > 0$) while continuing circulation of process tap water in the base pedestal. Thus, in this study, the initial concentration of solute in the base pedestal was maintained at zero (*i.e.* $C_{ob} = 0$).

The circulation outflow from the bottom of the specimen was also collected and subsequently analyzed for electrical conductivity (EC), chloride (Cl^-) concen-

https://doi.org/10.1346/CCMN.2003.0510209 Published online by Cambridge University Press

trations using ion chromatography, and calcium (Ca^{2+}) concentrations using inductively coupled plasma (detection via atomic emission spectrometry). At the end of the experiment, which lasted ~75 days, the cell was disassembled, and the final thickness and porosity of the specimen were measured.

RESULTS AND DISCUSSION

Electrical conductivities

The electrical conductivities measured in the circulation outflows from the top and bottom boundaries during the chemico-osmotic/diffusion stage of the experiment are shown in Figure 5. The electrical conductivity in the circulation outflow from the top boundary of the specimen, EC_{top}, was maintained relatively constant at a value of slightly greater than 100 mS/m. However, the electrical conductivity of the circulation outflow from the bottom boundary, $EC_{botttom}$, gradually increases from ~4 mS/m immediately after the start of the chemico-osmotic/diffusion stage to ~20 mS/m at ~30 to 35 days after the start of the chemico-osmotic stage. These measured EC values reflect the boundary conditions imposed in the experiment. For example, the lower EC_{top} relative to the source solution (*i.e.* $EC_{top} < 121$ mS/m) is consistent with the loss of solute mass from the source solution due to diffusion into the specimen, whereas the eventual increase in EC_{bottom} with time is consistent with the gain of solute mass in the bottom circulation outflow due to diffusion through the specimen. The establishment of steady EC_{bottom} values of ~20 mS/m ~30 to 35 days after the start of the chemico-osmotic stage of the experiment is consistent with the establishment of steady-state diffusion of $CaCl_2$ through the specimen.

Membrane efficiency

The induced pressure difference, $-\Delta P$ (> 0), across the GCL specimen and the corresponding membrane efficiency in the form of the chemico-osmotic efficiency coefficient, ω, are plotted *vs.* time in Figure 6 (note: values of ΔP and $\Delta\pi$ are < 0 because pressure increases in the negative x direction, or upward; see Figure 2). The values of ω in Figure 6 were calculated using equation 1, the measured induced pressure differences, and a chemico-osmotic pressure, $\Delta\pi$, of −36.9 kPa in accordance with equation 3 using $\nu = 3$ for $CaCl_2$ and $\Delta C = -0.005$ M $CaCl_2$.

A slight induced pressure difference was observed during the initial 5-day stage where processed tap water was circulated through both porous stones such that a concentration gradient was not applied across the specimen. This pressure difference has been attributed, in part, to slightly different hydraulic resistances of the two porous stones such that the head losses in each stone are not exactly the same, typically resulting in a slight recorded pressure difference across the specimen (Malusis *et al.*, 2001b; Malusis and Shackelford, 2002a). However, the induced pressure difference at the end of this 5-day flushing stage was negligible, as shown in Figure 6.

Immediately after replacing the processed tap water circulating across the top of the specimen with the 5 mM $CaCl_2$ solution (*i.e.* at $t = 0$), the induced pressure difference increases immediately and continues to increase gradually to a maximum value of ~19.3 kPa after 9 days corresponding to a maximum chemico-osmotic efficiency coefficient, ω_{max}, of 0.52 or membrane efficiency of 52%. Thereafter, the induced pressure difference and corresponding membrane efficiency gradually decrease such that the observed membrane behavior is effectively destroyed after 35 days.

Short-circuiting of the specimen, *e.g.* in terms of side-wall leakage (see Shackelford, 1994), is not likely in this experiment for the following reasons: (1) solution flow through the specimen, which is a prerequisite in most studies showing side-wall leakage, was prevented during the chemico-osmotic stage of the experiment; (2) the electrolyte concentration (5 mM $CaCl_2$) used in the experiment is low, and certainly lower than the vast

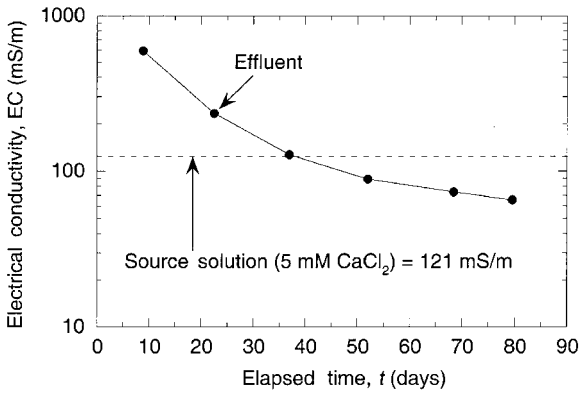


Figure 4. Electrical conductivity of effluent from specimen resulting from permeating specimen with processed tap water prior to the chemico-osmotic stage of the experiment.

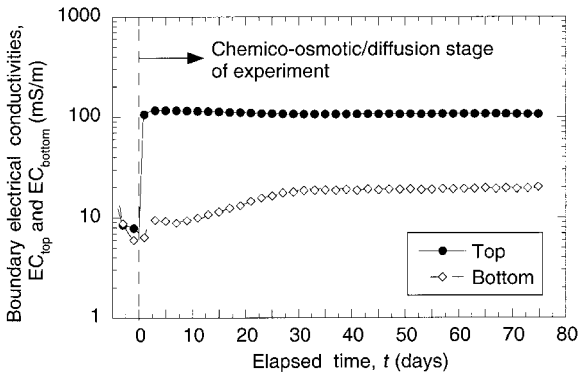


Figure 5. Electrical conductivities of circulation outflows from top and bottom boundaries of specimen during chemico-osmotic stage of experiment.

https://doi.org/10.1346/CCMN.2003.0510209 Published online by Cambridge University Press

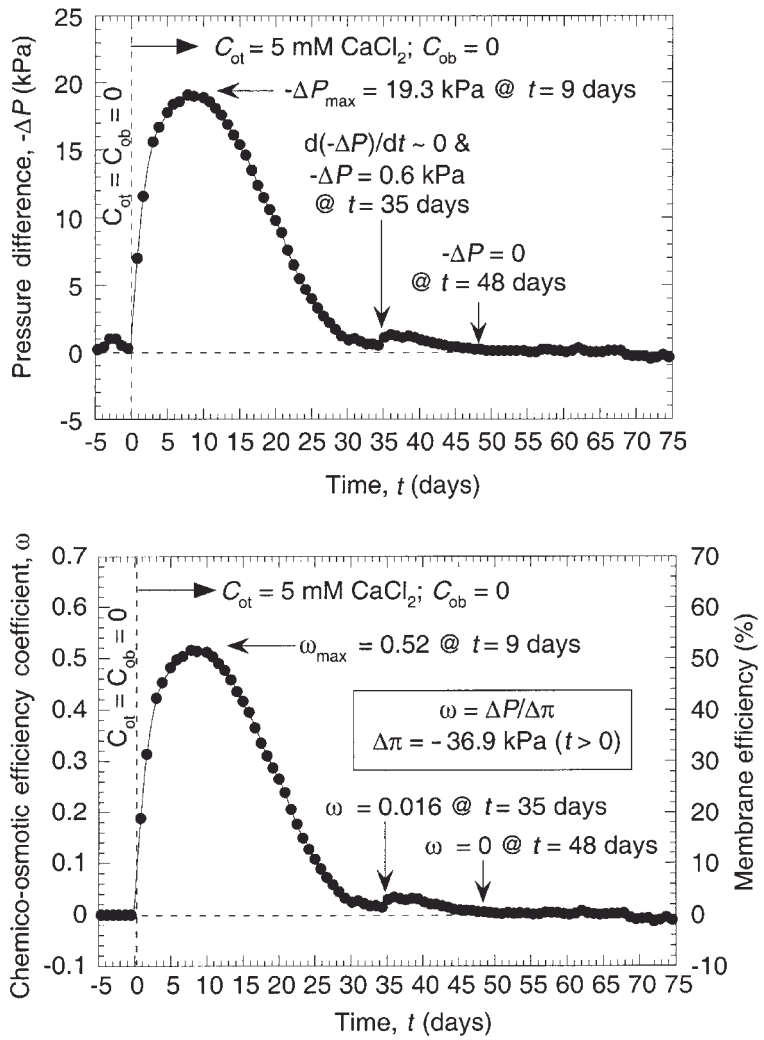


Figure 6. Measured induced chemico-osmotic pressure difference and calculated chemico-osmotic efficiency as a function of time.

majority of cases in which side-wall leakage has been reported; (3) the swelling pressure of the specimen was probably sufficiently high to prevent shrinkage, and no physical evidence of shrinkage after breakdown of the test apparatus was observed; and (4) a much more rapid diminishing of the induced chemico-osmotic pressure difference than was observed would be expected had specimen shrinkage, if any, been significant. Instead, the gradual post-peak decrease in $-\Delta P$ with time, shown in Figure 6, suggests that the response of the specimen to the imposed boundary conditions is due to a naturally occurring, physico-chemical process, such as collapse of the diffuse double layers (DDLs) due to an increase in the Ca^{2+} concentration in the pore-water of the specimen, which is consistent with previous conclusions (Barbour, 1986; Barbour and Fredlund, 1989; Whitworth and Fritz, 1994; Malusis *et al.*, 2001b; Malusis and Shackelford, 2002a). However, unlike previous studies whereby an increase in salt concentration in the pore-water of the specimen resulted in only a partial reduction in the observed membrane efficiency during the test, the divalent calcium concentration (5 mM Ca^{2+}) used in this study was apparently sufficiently strong to completely destroy the tendency of the GCL specimen to behave as a semipermeable membrane. Since the migration of Ca^{2+} is due solely to diffusion, the time required for complete destruction of the observed membrane behavior should be reasonably correlated with the time required to reach steady-state diffusion of the Ca^{2+}.

Solute diffusion

The measured chloride (Cl^-) and calcium (Ca^{2+}) concentrations in the circulating liquid exiting the base pedestal are plotted *vs.* time in Figure 7. The corresponding values of cumulative mass per unit area, Q_t, based on the Cl^- and Ca^{2+} concentrations calculated in accordance with equation 4 are plotted *vs.* time in Figure 8.

The scatter in the measured Cl^- concentration data masks somewhat the existence of steady-state conditions

https://doi.org/10.1346/CCMN.2003.0510209 Published online by Cambridge University Press

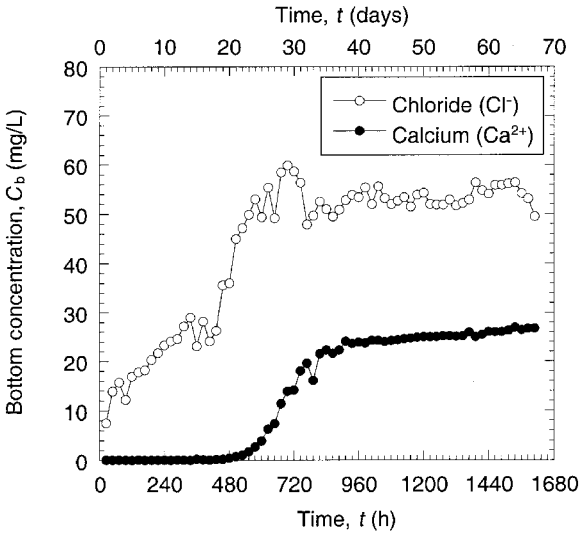


Figure 7. Measured chloride and calcium concentrations exiting the base pedestal of the test cell due to diffusion.

with respect to diffusion of the Cl^-, and the Ca^{2+} concentration data appear to be increasing, albeit slightly, even after 68 days of monitoring, suggesting that steady-state diffusion of Ca^{2+} was approached, but not necessarily established. As a result, the time required to reach steady-state diffusion was evaluated in a more systematic manner by performing sequential linear regression analyses on an increasing number of Q_t *vs.* t data, starting from an analysis performed using only the last 2 data points, followed by subsequent linear regression analyses on an increasing number of data (*i.e.* adding one additional datum for each subsequent analysis) until all of the data were used in an analysis. Therefore, since 67 samples were collected during the test at a rate of one per day, a total of 66 linear regression analyses were performed for each solute.

The coefficient of determination, r^2, resulting from each regression analysis is plotted as a function of the number of data used in the analysis for both Cl^- and Ca^{2+} in Figure 9. The number of data corresponding to the location where r^2 starts to deviate significantly from unity is taken as the transition from a non-linear to linear slope in the Q_t *vs.* t data corresponding to the transition from the transient portion of the data to the steady-state portion of the data. Accordingly, the times corresponding to the earliest data used in each regression analysis also are plotted *vs.* the corresponding r^2 values in Figure 9.

As shown in Figure 9, the r^2 values based on the regression analyses using the Q_t *vs.* t data for Cl^-

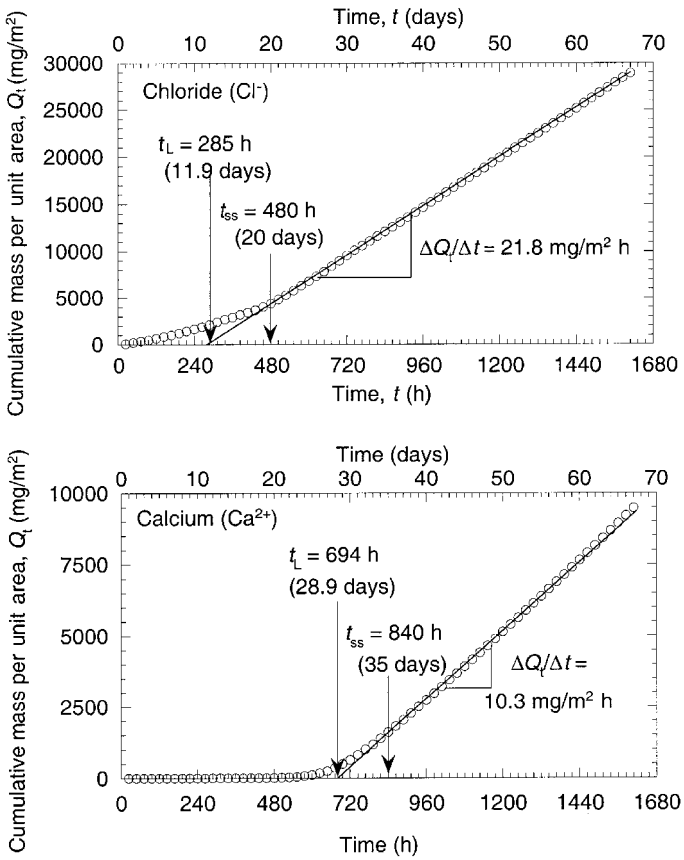


Figure 8. Cumulative mass data based on measured bottom concentrations (t_L = time lag; t_{ss} = time to steady-state diffusion).

https://doi.org/10.1346/CCMN.2003.0510209 Published online by Cambridge University Press

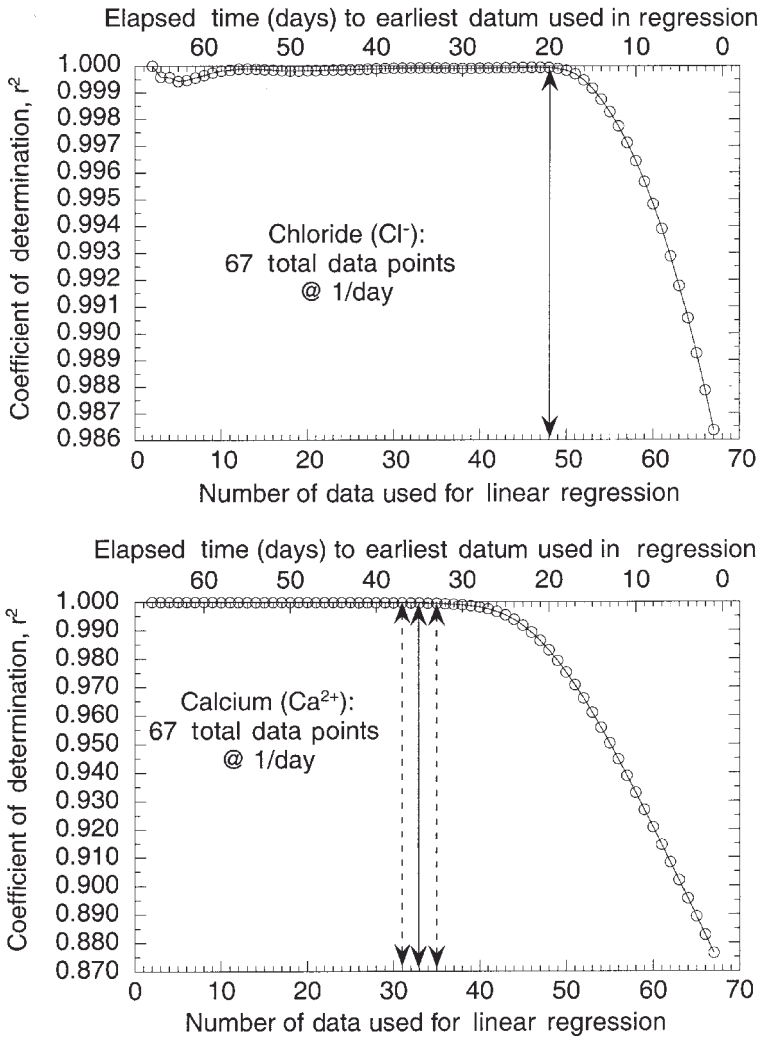


Figure 9. Coefficients of determination from multiple linear regression analyses performed on measured cumulative mass data as a function of the number of data used for linear regression and the elapsed time to the earliest datum used in the regression.

decrease dramatically when more than 48 data are used in the analysis. Thus, the elapsed time associated with the earliest of the 48 data points used in the analysis represents the time at which steady-state diffusion of Cl^- is established; *i.e.* t_{ss} is 20 days for Cl^-. Although this distinction is not quite as evident in the results based on the Q_t *vs.* t data for Ca^{2+}, the use of 33±2 data corresponding to t_{ss} of 35±2 days appears reasonable for Ca^{2+}.

The time lag, t_L, and slope of the steady-state portion of the data for each solute shown in Figure 8 are based on the results of the linear regression analyses using 48 Q_t *vs.* t data for Cl^- and 33 Q_t *vs.* t data for Ca^{2+}. The higher t_L of 694 h (28.9 days) for Ca^{2+} relative to the t_L of 285 h (11.9 days) for Cl^- is attributed to the tendency for cation exchange associated with the divalent calcium cation (*e.g.* Malusis *et al.*, 2001b).

At steady state, electroneutrality requires that the charge flux of the Cl^- has the same magnitude as the charge flux of the Ca^{2+}. This requirement may be written as follows:

$$J_{Cl^-}|z_{Cl^-}| = J_{Ca^{2+}}|z_{Ca^{2+}}| \quad (6)$$

where J_{Cl^-} and $J_{Ca^{2+}}$ = the steady-state diffusive molar fluxes of Cl^- and Ca^{2+}, and z_{Cl^-} and $z_{Ca^{2+}}$ = the charges Cl^- and Ca^{2+} (*i.e.* −1 and +2, respectively). Therefore, the steady-state diffusive molar flux of Cl^- theoretically should be twice the magnitude of the steady-state diffusive molar flux of Ca^{2+}. In terms of mass fluxes, this ratio must be multiplied by the ratio of the atomic weight of Ca^{2+} (40.08) to the atomic weight of Cl^- (35.453). Therefore, the magnitude of the steady-state diffusive mass flux of Cl^- theoretically should be 2.26 [= $2 \times (40.08/35.453)$] times the magnitude of the steady-state diffusive mass flux of Ca^{2+}. Based on the results shown in Figure 8, the observed ratio of the steady-state diffusive mass flux of Cl^- to the steady-state diffusive mass flux of Ca^{2+} in this study is 2.11

https://doi.org/10.1346/CCMN.2003.0510209 Published online by Cambridge University Press

(= 21.8/10.3), which is sufficiently close to the theoretical value of 2.26 to suggest that steady-state diffusion of Ca^{2+} had essentially been established.

Finally, the effective diffusion coefficients, D^*, for Cl^- and Ca^{2+} calculated in accordance with equation 5 using a measured porosity (n) of 0.718 and an averaged measured thickness (L) of 5.6 mm are 1.21×10^{-10} m^2/s and 1.10×10^{-10} m^2/s, respectively. The closeness in these D^* values also is consistent with the electroneutrality constraint that requires the two D^* values to be the same at steady-state diffusion.

Conceptual explanation

The t_{ss} of 35±2 days for Ca^{2+} is identical to the time required for effective destruction of the observed membrane behavior, as indicated in Figure 6. Thus, the correlation between the times required for effective destruction of the membrane behavior and the establishment of steady-state diffusion of the Ca^{2+} is excellent. Therefore, the results of this study provide the first direct evidence that complete destruction of clay membrane behavior can be caused by diffusion of the principal salt cation (*i.e.* Ca^{2+}). However, because clay membranes by definition restrict solute migration, the question as to how this migration can occur is raised.

A conceptual explanation for the observed correlation between Ca^{2+} diffusion and the destruction of the observed membrane behavior of the GCL can be formulated on the basis of the clay structure models described by Pusch (1999) and Pusch and Schomburg (1999). In these models, the bentonite consists of an intermingled structure of both unit particles and particle clusters, with the primary pores located between the unit particles and the clusters. At the measured porosity of the specimen of 0.718, interlayer spacing of the particles will be controlled by surface hydration rather than by the diffuse double layer interactions, such that the interlayer spacing of the unit particles will probably not have been affected much by the exchangeable cation (*e.g.* van Olphen 1977). However, diffuse double layers will probably have extended into the voids between both unit particles and particle clusters, thereby restricting the diffusive migration of the ions. In this case, the destruction of the observed membrane behavior can be explained in terms of decreasing diffuse double layer thickness between unit particles and particle clusters with increasing pore concentration due to ion diffusion, resulting in a gradual destruction of the observed membrane behavior.

CONCLUSIONS

The results of a combined chemico-osmotic/diffusion experiment conducted on a geosynthetic clay liner containing Na-bentonite and exposed to a constant concentration difference of 5 mM $CaCl_2$ show an initial increase in induced pressure difference across the specimen to a maximum value of 19.3 kPa corresponding to a maximum membrane efficiency of 52% after 9 days of testing. This membrane behavior observed initially is followed by a gradual decrease in induced pressure difference to almost zero (0.6 kPa) corresponding to a membrane efficiency of only 1.6% after 35 days of testing, and subsequently to zero after 48 days of testing. The effective destruction of the initially observed semipermeable membrane behavior after 35 days of testing correlates well with the time of 35±2 days required to essentially achieve steady-state Ca^{2+} diffusion. This correlation suggests that the decrease in induced pressure difference is consistent with compression of diffuse double layers between clay particles and particle clusters due to diffusion of Ca^{2+}, resulting in concomitant increase in pore sizes and decrease in the membrane efficiency. The results illustrate the potentially destructive role of diffusion of invading salt cations on the membrane behavior of clays, and are particularly relevant with respect to the ability of clays to sustain membrane behavior.

ACKNOWLEDGMENTS

The authors are indebted to Doug Stewart of the University of Leeds (UK) for providing insight into the conceptual explanation described in this paper. Financial support for this study was provided by the US National Science Foundation (NSF), Arlington, Virginia, under Grant CMS-9820863 entitled, "Long-Term Performance of GCLs Permeated with Aqueous Inorganic Solutions". The opinions expressed in this paper are solely those of the writers and are not necessarily consistent with the policies or opinions of the NSF.

REFERENCES

Barbour, S.L. (1986) *Osmotic Flow and Volume Change in Clay Soils*. Ph.D. dissertation, University of Saskatchewan, Saskatoon, Saskatchewan, Canada.

Barbour, S.L. and Fredlund, D.G. (1989) Mechanisms of osmotic flow and volume change in clay soils. *Canadian Geotechnical Journal*, **26**, 551–562.

Fritz, S.J. (1986) Ideality of clay membranes in osmotic processes: A review. *Clays and Clay Minerals*, **34**, 214–223.

Groenevelt, P.H. and Elrick, D.E. (1976) Coupling phenomena in saturated homo-ionic montmorillonite: II. Theoretical. *Soil Science Society of America, Journal*, **40**, 820–823.

Hanshaw, B.B. and Coplen, T.B. (1973) Ultrafiltration by a compacted clay membrane – II. Sodium ion exclusion at various ionic strengths. *Geochimica et Cosmochimica Acta*, **37**, 2311–2327.

Katchalsky, A. and Curran, P.F. (1965) *Nonequilibrium Thermodynamics in Biophysics*. Harvard University Press, Cambridge, Massachusetts, 248 pp.

Keijzer, Th.J.S. and Loch, J.P.G. (2001) Chemical osmosis in compacted dredging sludge. *Soil Science Society of America, Journal*, **65**, 1045–1055.

Keijzer, Th.J.S., Kleingeld, P.J. and Loch, J.P.G. (1997) Chemical osmosis in compacted clayey material and the prediction of water transport. Pp. 199–204 in: *Geoenvironmental Engineering, Contaminated Ground: Fate of Pollutants and Remediation* (R.N. Yong and H.R.

https://doi.org/10.1346/CCMN.2003.0510209 Published online by Cambridge University Press

Thomas, editors). Thomas Telford Publishers, London.
Keijzer, Th.J.S., Kleingeld, P.J. and Loch, J.P.G. (1999) Chemical osmosis in compacted clayey material and the prediction of water transport. *Engineering Geology*, **53**, 151–159.
Kemper, W.D. and Quirk, J.P. (1972) Ion mobilities and electric charge of external clay surfaces inferred from potential differences and osmotic flow. *Soil Science Society of America, Proceedings*, **36**, 426–433.
Kemper, W.D. and Rollins, J.B. (1966) Osmotic efficiency coefficients across compacted clays. *Soil Science Society of America, Proceedings*, **30**, 529–534.
Malusis, M.A. and Shackelford, C.D. (2002a) Chemico-osmotic efficiency of a geosynthetic clay liner. *Journal of Geotechnical and Geoenvironmental Engineering*, **128**, 97–106.
Malusis, M.A. and Shackelford, C.D. (2002b) Coupling effects during steady-state solute diffusion through a semipermeable clay membrane. *Environmental Science and Technology*, **36**, 1312–1319.
Malusis, M.A., Shackelford, C.D. and Olsen, H.W. (2001a) Flow and transport through clay membrane barriers. Pp. 334–341 in: *Geoenvironmental Engineering: Geoenvironmental Impact Management* (R.N. Young and H.R. Thomas, editors). Thomas Telford Publishers, London.
Malusis, M.A., Shackelford, C.D. and Olsen, H.W. (2001b) A laboratory apparatus to measure chemico-osmotic efficiency coefficients for clay soils. *Geotechnical Testing Journal*, **24**, 229–242.
Olsen, H.W., Yearsley, E.N. and Nelson, K.R. (1990) Chemico-osmosis versus diffusion-osmosis. *Transportation Research Record No. 1288*. Transportation Research Board, Washington D.C., pp. 15–22.
Pusch, R. (1999) Microstructural evolution of buffers. *Engineering Geology*, **54**, 33–41.
Pusch, R. and Schomburg, J. (1999) Impact of microstructure on the hydraulic conductivity of undisturbed and artificially prepared smectitic clays. *Engineering Geology*, **54**, 167–172.
Shackelford, C.D. (1991) Laboratory diffusion testing for waste disposal – A review. *Journal of Contaminant Hydrology*, **7**, 177–217.
Shackelford, C.D. (1994) Waste-soil interactions that alter hydraulic conductivity. Pp. 111–168 in: *Hydraulic Conductivity and Waste Contaminant Transport in Soil,* ASTM STP 1142, (D.E. Daniel and S.J. Trautwein, editors). ASTM, West Conshohoken, Pennsylvania.
Shackelford, C.D. and Daniel, D.E. (1991) Diffusion in saturated soil: I. Background. *Journal of Geotechnical Engineering*, **117**, 467–484.
Shackelford, C.D. and Redmond, P.L. (1995) Solute breakthrough curves for processed kaolin at low flow rates. *Journal of Geotechnical Engineering*, **121**, 17–32.
Shackelford, C.D., Malusis, M.A. and Olsen, H.W. (2001) Clay membrane barriers for waste containment. *Geotechnical News*. BiTech Publishers, Richmond, British Columbia, Canada, **19**, 39–43.
Staverman, A.J. (1952) Non-equilibrium thermodynamics of membrane processes. *Transactions of the Faraday Society*, **48**, 176–185.
van Olphen, H. (1977) *An Introduction to Clay Colloid Chemistry*, 2nd edition. John Wiley and Sons, Inc., New York, 318 pp.
van Oort, E., Hale, A.H., Mody, F.K. and Roy, S. (1996) Transport in shales and the design of improved water-based shale drilling fluids. *SPE Drilling and Completion*, **11**, 137–146.
Whitworth, T.M. and Fritz, S.J. (1994) Electrolyte-induced solute permeability effects in compacted smectite membranes. *Applied Geochemistry*, **9**, 533–546.

(*Received 7 August 2002; revised 20 November 2002; Ms. 706*)

https://doi.org/10.1346/CCMN.2003.0510209 Published online by Cambridge University Press